Fuel 230 (2018) 266–273

Contents lists available at ScienceDirect

Fuel

journal homepage: www.elsevier.com/locate/fuel

Full Length Article

Paraffin solubility curves of diesel fuels from thermodynamic model adjusted through experimental DSC thermograms

Rafael P. do Carmo[a], Vinicius M. da Silva[b], Felipe P. Fleming[c,d,e], Jean-Luc Daridon[d], Jérôme Pauly[d], Frederico W. Tavares[a,b,*]

[a] Programa de Engenharia Química/COPPE – Universidade Federal do Rio de Janeiro, Cidade Universitária, Rio de Janeiro, RJ, Brazil
[b] Escola de Química, Universidade Federal do Rio de janeiro, Cidade Universitária, Rio de Janeiro, RJ, Brazil
[c] CENPES – Centro de Pesquisas da Petrobras, Cidade Universitária, Rio de janeiro, RJ, Brazil
[d] LFC-R, IPRA, UMR5150, CNRS/TOTAL/Univ Pau & Pays Adour, 64000 Pau, France
[e] Programa de Engenharia Mecânica, PUC-RIO, Rio de Janeiro, RJ, Brazil

ARTICLE INFO

Keywords:
Diesel
Paraffin
DSC
Experimental data
Solid-liquid equilibria

ABSTRACT

DSC and wax solubility curves were measured for two diesel fuel samples. Compositional profiles were also measured for the solubility curve points. The paraffin distributions of the samples were determined and the non-paraffinic components were lumped into pseudocomponents. The liquid phase was modeled using the Peng-Robinson equation of state with the classical van der Waals mixing rule. For the solid phase, the modified UNIQUAC model was employed. The models were fitted to the DSC data by tuning only four multipliers acting on the molecular weights, boiling and critical temperatures of the pseudocomponents as well as on the paraffins' pair interaction energies from the UNIQUAC model. Then the model is used to predict wax appearance temperature, amount and composition of solid deposit as a function of temperature during cooling. Excellent results were obtained for the two samples analyzed. This way, the methodology developed is able to predict adequately the formation of solid paraffin from diesel fuels.

1. Introduction

Diesel fuels are widely used on road, marine and air transports. These fuels are composed in great part by paraffins, which crystallize and form gels when submitted to low temperatures. Consequently, it reduces the fuel flow by plugging the fuel filters [1] and, as the fuel fluid composition is altered by the precipitation, jeopardizes the engine efficiency [2,3]. To avoid these issues, paraffin precipitation is usually controlled by using additives in the fuels [2,3].

Simulation of the diesel phase behavior may help determining how much additive should be used to avoid paraffin solidification in a desired temperature range. Different models have been used to model solid paraffin solubility curves from diesel fuels, as these curves are extremely laborious to measure experimentally. Coutinho et al. [4] and Sansot et al. [5] used an equation of state for the liquid phase and the modified Wilson model for the solid phase. Coutinho et al. [6] and Coutinho [1] employed the combination of the UNIFAC model and the Flory free volume equation for the liquid phase and the modified UNIQUAC model for the solid phase. To tune these models, the wax appearance temperature (WAT) was majorly employed. Nevertheless, all current experimental techniques available to measure the WAT have shortcomings that limits an effective measurement of the thermodynamic equilibrium temperature [7]. The supersaturation unavoidable in WAT measurements due to kinetic effects also imposes limitations to its use in model tuning.

To avoid such interferences, a different approach has been recently proposed [8,9]. In this new approach, the single WAT point commonly used to tune the thermodynamic model is substituted by an entire DSC thermogram, that provides phase equilibria information over a large temperature range. Using an appropriate cooling rate in the DSC experiments, solid-liquid equilibrium data is indirectly provided via the enthalpy variation of the system and can thus be directly calculated through an appropriate thermodynamic model. Nevertheless, this approach has only been applied so far to synthetic systems where the composition was controlled and well known. The aim of the present work is to extend the method do Diesel fuels and improve the reliability of paraffin solubility curves obtained from thermodynamic models.

For that purpose, experimental DSC and experimental solubility data were measured for two different Diesel fuel samples. These samples compositions were then analyzed and characterized by their full

* Corresponding author at: Programa de Engenharia Química/COPPE – Universidade Federal do Rio de Janeiro, Cidade Universitária, Rio de Janeiro, RJ, Brazil.
E-mail address: tavares@eq.ufrj.br (F.W. Tavares).

https://doi.org/10.1016/j.fuel.2018.05.063
Received 10 March 2018; Received in revised form 9 May 2018; Accepted 12 May 2018
Available online 25 May 2018
0016-2361/ © 2018 Elsevier Ltd. All rights reserved.

Nomenclature

h	*molar enthalpy*
T	temperature
P	pressure
N_c	number of components
N_p	number of phases
$N_p araf$	number of paraffins
N_{pseudo}	number of pseudocomponents
N_{mol}	number of moles
C_p	heat capacity
x	mole fraction
f	fugacity
m	EoS parameter
Kw	Watson factor
r,q	structural parameters
Z	coordination number
R	universal gas constant
Q	heat
t	time

Superscripts and Subscripts

fus	fusion
tr	crystalline transition
sub	sublimation
vap	vaporization
ig	ideal gas
c	critical
b	boiling
L	liquid
S	solid
R	residual
E	excess
exp	experimental
i,j	index
l	pseudocomponents index

Greek letters

Δ	variation
γ	activity coefficient
τ,θ,ϕ	modified UNIQUAC parameters
λ	pair interaction energy
φ	fugacity coefficient
ρ	density
ω	acentric factor
β	phase fraction
ξ	estimated parameter

Accent

$\overline{M}$	average property M (M is a dummy variable)
$\underline{M}$	vector M
$\widehat{M}$	property M in the mixture

Abbreviations

PR-EoS	Peng-Robinson equation of state
SLE	solid-liquid equilibrium
CN	carbon number
MW	molecular weight
SG	specific gravity at 15.5 °C
WAT	wax appearance temperature

paraffin distributions whereas non-paraffinic components were lumped into pseudocomponents. The Peng-Robinson equation of state (PR-EoS) was used to model the liquid phase, as it can be readily applied to high pressures systems and complex fluids like crude oil. For the solid phase, the modified UNIQUAC model was used. The models were tuned using the calorimetric data and the predictions obtained for the solubility and compositional data were analyzed.

2. Experimental

2.1. Diesel samples

The two samples used in this study were supplied by PETROBRAS and used without any further treatment. Density, Flash Point and Sulfur content of the two samples are presented in Table 1.

2.2. DSC measurements

The calorimetric experiments were carried out using a SETARAM Micro DSC 7 evo calorimeter. All experiments were performed using a temperature rate of 0.2 K.min^{-1} in, at least, triplicates. Samples of around 450 mg were weighted with a precision of 0.01 mg. The experiments were conducted at temperatures from 248.15 K to 303.15 K. The equipment was calibrated using Gallium. This reference compound was acquired from Fluka as an ultrapure sample (purity of 99.999%).

2.3. Analysis of the paraffin distributions

The paraffin distribution within the samples were analyzed using gas chromatography. An Agilent 6890 chromatograph equipped with a split/splitless injector, a flame ionization detector (FID) and HP-1 50 m capillary column with an internal diameter of 0.20 mm and a film width of 0.11 μm was used. The carrier gas used was hydrogen at a constant pressure of 25 psi. The injector temperature was kept constant at 573.15 K and a split ratio of 128:1 was used. The detector was kept at a constant temperature of 573.15 K with constant flow of air (450 mL.min^{-1}). The column temperature was raised from 313.15 K to 573.15 K at 2 K.min^{-1} and from there raised to 653 K at 4 K.min^{-1}. The sample was diluted in CS_2 and 1 μL of the solution was injected using an automatic injection system. The retention time of the different *n*-alkanes were calibrated using a standard mixture Polywax 655 from Supelco. Each sample was injected in at least triplicates. The uncertainties calculated from two standard deviations of the results were smaller than 2% for all cases. *n*-alkanes up to C35 were identified.

2.4. Analysis of fluid composition and fluid representation

The total composition of the sample was represented by discretizing the original samples into pseudocomponents characterized by their average carbon number and subtracting from each of them the corresponding concentration of paraffin analyzed.

The method used is based on the ASTM standard 7169. An Agilent 6890 N chromatograph equipped with an on-column injector, a FID

Table 1
Density, Flash Point and Sulfur content of the two samples studied.

Sample	Density (kg.m^{-3})	Flash Point (°C)	Sulfur content (ppm)
1	828.2	68.0	1.6
2	824.5	69.0	0.9

Viance Exhibit 1068
Viance v. Koppers Performance Chemicals
PGR2026-00023
Page 2 of 8

detector and 5 m steel capillary column with an internal diameter of 0.53 mm and a film width of 0.09 μm was used. The carrier gas used was helium at 25 mL.min^{-1}. The injector temperature was raised from 373.15 K to 703.15 K at 15 K.min^{-1} and is then kept constant for 26 min. The detector was kept at a constant temperature of 703.15 K with constant flows of hydrogen (35 mL.min^{-1}) and air (350 mL.min^{-1}). The column temperature was raised from 308.15 K to 703.15 K at 10 K.min^{-1} and is then kept constant for 5 min. The sample was diluted in CS_2 and 0.5 μL were injected using an automatic injection system. The retention time of the different *n*-alkanes were calibrated using a standard mixture Polywax 655 from Supelco. Each sample was injected in at least triplicates. The uncertainties calculated from two standard deviations of the results were smaller than 3% for all cases. *n*-alkanes up to C35 were identified.

2.5. Solubility curve and solid deposit composition

In addition to the calorimetric measurements used for tuning the model, solid liquid phase behavior was studied below the onset of wax crystallization by measuring both the solubility curve and the composition of the waxy solid deposit as a function of temperature. These measurements which are not needed for the implementation of the method were used in the present work only to test the predictive capacity of the proposed method. The solubility curve of both Diesel fuels were measured using a centrifugation method similar to the one proposed by Han et al. [10]. The method consists of cooling the sample to a controlled temperature of interest and proceed a centrifugation at that temperature. The centrifuged sample is then separated in two fractions. The first fraction contains only liquid without the presence of any solids whatsoever. The second fraction contains all of the precipitated solid paraffin and some of the liquid. If one ignores the effect of the centrifugation field on the phase equilibrium of the system, one may assume that the fractions are in equilibria, and consequently the liquid in the first fraction has the same composition of the liquid that remained in the second fraction. Each of these fractions were only analyzed for their paraffin distributions following the method detailed above.

Assuming that the solids are only composed by paraffins, one can use the paraffin distribution of the first fraction and subtract the paraffins that are present on the second fraction due to the presence of the liquid phase and calculate the paraffin composition of the solid wax and consequently its mass. The calculations were carried out as described by Han et al. [10] and Coutinho et al. [6].

The centrifugations were performed in a THERMO Heraeus Megafuge 40R centrifuge. The samples were disposed in small flasks containing 1 g of sample each. For each temperature and each Diesel sample, three flasks were centrifuged. Together with the samples flasks, an extra flask holding kerosene was added and before the samples were fractionated the temperature of the kerosene flask was measured with a 0.1 K precision thermometer and reported as the equilibrium temperature.

Mass losses at the fractionation step were always smaller than 0.1% of the total mass of the sample. Combined with the uncertainties from the chromatographic analyzes, the expanded uncertainties of each solubility curve point measured are estimated as 5% of the mass of the solid paraffin.

3. Methodology

3.1. Thermodynamic model

The solid-liquid equilibrium was calculated by means of the following equation

$$x_i^{\mathrm{L}}\hat{\varphi}_i^{\mathrm{L}}P = x_i^{\mathrm{S}}\gamma_i^{\mathrm{S}}f_i^{\mathrm{S}} \tag{1}$$

which represents, for each component i, the equality between its fugacity in the liquid phase, $\hat{f}_i^{\mathrm{L}}$, and in the solid phase, $\hat{f}_i^{\mathrm{S}}$. In Eq. (1), x, f, $\hat{\varphi}$ and γ are the composition, the fugacity of pure component, the fugacity coefficient in a mixture and the activity coefficient. It was considered that only the paraffins can precipitate, that is, the pseudocomponents are present only in the liquid phase.

The fugacity coefficients in the liquid phase were calculated using the Peng-Robinson equation of state with the classical van der Waals combining rules, in which all the binary interaction parameters, k_{ij}, were set to zero. The critical temperature, T_c, critical pressure, P_c, and acentric factor, ω, were obtained for each paraffin i through the correlations proposed by Marano and Holder [11], presented in Eqs. (2), (3) and 4, respectively.

$$T_c i(K) = 1020.71-(1020.71-127.89)\exp(-0.1981(\mathrm{CN}_i-0.896021)^{0.629752}) \tag{2}$$

$$P_{ci}(bar) = 1336.74\exp(-2.111827(\mathrm{CN}_i + 3.625581)^{0.258439}) \tag{3}$$

$$\omega_i = -6.5597 + 3.383261(\mathrm{CN}_i + 23.608415)^{0.20877} \tag{4}$$

For each pseudocomponent l, T_c, P_c and ω were calculated using the correlations proposed by Pedersen and Christensen [12], presented in Eqs. 5, 6, 7 and 8 respectively. The densities of the pseudocomponents, ρ, and their molecular weights MW, were obtained from Katz and Firoozabadi [13].

$$T_{cl}(K) = 73.4043\rho_l + 97.3562\ln\mathrm{MW}_l + 0.618744\mathrm{MW}_l + \frac{-2059.32}{\mathrm{MW}_l} \tag{5}$$

$$\ln P_{cl}(bar) = 0.0728462\rho_l + 2.18811\rho_l^{0.25} + \frac{163.910}{\mathrm{MW}_l} + \frac{-4043.23}{\mathrm{MW}_l^2} \tag{6}$$

$$m_l = 0.373765 + 0.00549269\mathrm{MW}_l + 0.017934\rho_l + 0.00000493049\mathrm{MW}_l^2 \tag{7}$$

$$m_l = 0.37464 + 1.54226\omega_l-0.26992\omega_l^2 \tag{8}$$

The activity coefficients of the components in the solid phase were calculated using the modified UNIQUAC model, proposed by Coutinho et al. [4], as shown in Eq. (9), in which Φ, θ and τ are obtained through Eqs. 10, 11 and 12, respectively.

$$\ln\gamma_i^S = \ln\left(\frac{\Phi_i}{x_i^s}\right) + 1-\frac{\Phi_i}{x_i^s}-\frac{Z}{2}q_i\left(\ln\left(\frac{\Phi_i}{\theta_i}\right) + 1-\frac{\Phi_i}{\theta_i}\right) + q_i-q_i\ln\left(\sum_{j=1}^{N_c}\theta_j\tau_{ji}\right) -q_i\sum_{j=1}^{N_c}\frac{\theta_j\tau_{ij}}{\sum_{k=1}^{N_c}\theta_k\tau_{kj}} \tag{9}$$

$$\Phi_i = \frac{x_i^{\mathrm{S}}r_i}{\sum_{j=1}^{N_c}x_j^{\mathrm{S}}r_j} \tag{10}$$

$$\theta_i = \frac{x_i^{\mathrm{S}}q_i}{\sum_{j=1}^{N_c}x_j^{\mathrm{S}}q_j} \tag{11}$$

$$\tau_{ji} = \exp\left(-\frac{\lambda_{ji}-\lambda_{ii}}{q_i RT}\right) \tag{12}$$

The parameters r_i, q_i and λ_{ii} (pair interaction energy) are calculated according to Eqs. 13, 14 and 15.

$$r_i = 0.6744\mathrm{CN}_i + 0.4534 \tag{13}$$

$$q_i = 0.540\mathrm{CN}_i + 0.616 \tag{14}$$

$$\lambda_{ii} = -\frac{2}{Z}(\Delta h_i^{\mathrm{sub}}-RT) \tag{15}$$

The parameter λ_{ij} assumes the value of pair interaction energy of the paraffin with the lower Carbon Number (CN) in the pair ij. In Eq. (15), $\Delta h_i^{\mathrm{sub}}$ is the molar enthalpy of sublimation of paraffin

i

Viance Exhibit 1068
Viance v. Koppers Performance Chemicals
PGR2026-00023
Page 3 of 8

, calculated via Eq. (16), in which Δh_i^{tr}, Δh_i^{fus} and Δh_i^{vap} are the molar enthalpies of crystalline transition, fusion and vaporization of paraffin i. The latter is obtained according to the correlation proposed by Morgan and Kobayashi [14] and Δh_i^{tr} and Δh_i^{fus} are obtained as suggested by Coutinho et al. [4].

$$\Delta h_i^{sub} = \Delta h_i^{vap} + \Delta h_i^{fus} + \Delta h_i^{tr} \quad (16)$$

The fugacity of the pure paraffin i in the solid phase, f_i^S, is calculated using Eq. (17), in which f_i^L is the fugacity of pure paraffin i in the liquid phase, obtained via the PR-EoS. T_i^{fus} and T_i^{tr} are the temperatures of fusion and solid-solid (ordered-disordered) transition of paraffin i, calculated through the correlations suggested by Coutinho et al. [4]. ΔCp_i^{LS} is the difference between the heat capacities of paraffin i in the liquid and solid phases, calculated using the correlation proposed by Pedersen et al. [15].

$$f_i^S = f_i^L \exp\left[\frac{\Delta h_i^{fus}}{RT_i^{fus}}\left(1-\frac{T_i^{fus}}{T}\right) + \frac{\Delta h_i^{tr}}{RT_i^{tr}}\left(1-\frac{T_i^{tr}}{T}\right) - \frac{1}{RT}\int_{T_i^{fus}}^{T} \Delta Cp_i^{LS} dT + \frac{1}{R}\int_{T_i^{fus}}^{T} \frac{\Delta Cp_i^{LS}}{T} dT\right] \quad (17)$$

The Poynting factor was neglected in the calculation of f^S, as can be observed in Eq. (17), since the pressure was held equal to 1 bar during all experiments.

3.2. DSC thermogram simulation from the thermodynamic model proposed

The DSC thermograms were calculated according to the methodology proposed by Silva et al. [9]. The liquid phase molar enthalpy, h^L, was obtained through Eq. (18), that describes a thermodynamic path starting at an ideal gas (

ig

) reference system at T_0 and P_0, changing its temperature using the ideal gas heat capacities and adding the residual enthalpy at the desired T and P. The enthalpy of the ideal gas system at the reference conditions T_0 and P_0, $h^{ig}(T_0,P_0)$, is considered equal to zero.

$$h^L(T,P,\underline{x}^L) = \sum_{i=1}^{N_c} x_i^L \int_{T_0}^{T} Cp_i^{ig} dT + h^R(T,P,\underline{x}^L) \quad (18)$$

The ideal gas heat capacities of the paraffins were obtained through the correlation of Passut and Danner [16] modified by Silva et al. [9], and the residual enthalpy is calculated from the PR-EoS.

$$Cp_i^{ig} = 251.996[B_i + 2C_iT + 3D_iT^2 + 4E_iT^3 + 5F_iT^4], \quad (19)$$

in which the coefficients B, C, D, E and F are calculated using Eqs. 20–24.

$$B_i = -7.100555 \times 10^{-4}CN_i - 1.201093 \times 10^{-4} \quad (20)$$

$$C_i = 1.416221 \times 10^{-5}CN_i + 2.669830 \times 10^{-6} \quad (21)$$

$$D_i = -3.149971 \times 10^{-9}CN_i + 4.003664 \times 10^{-10} \quad (22)$$

$$E_i = 3.489865 \times 10^{-13}CN_i - 1.321624 \times 10^{-13} \quad (23)$$

$$F_i = -1.105366 \times 10^{-17}CN_i + 8.714208 \times 10^{-18} \quad (24)$$

The ideal gas heat capacities of the pseudocomponents were calculated using Eq. (25), proposed by Kesler and Lee [17]

$$Cp_l^{ig} = \frac{MW_l[A_0l + A_1lT + A_2lT^2 - B_3l(B_0l + B_1lT + B_2lT^2)]}{4.19002}, \quad (25)$$

in which the coefficients A_0, A_1, A_2, B_0, B_1, B_2 and C are obtained by means of Eqs. 26–32.

$$A_{0l} = -1.41779 + 0.11828Kw_l \quad (26)$$

Table 2
Feed compositions of both Diesel fuel samples divided into paraffins and other components lumped into pseudocomponents in mass fractions (%) and average MW (g.mol^{-1}). The relative extended uncertainty of the composition is under 2% for the paraffin components and under 3% for the pseudocomponents of the reported value. The relative extended uncertainty of the average molecular mass is 3%.

Carbon Number	1		2	
	Paraffin	Pseudocomp.	Paraffin	Pseudocomp.
7	0.0425	0.1648	0.0381	–
8	0.2675	0.3501	0.2739	0.6361
9	0.6065	1.8255	0.6904	2.0678
10	0.8774	3.6571	1.0023	4.2041
11	1.1587	5.5495	1.4262	5.9890
12	1.4446	6.5777	1.8173	7.3054
13	1.7070	8.2085	2.0958	9.0891
14	2.1668	7.9017	2.4777	8.9089
15	2.4542	7.8873	2.7530	7.6142
16	2.0144	5.9382	2.2158	5.7477
17	1.8993	6.5838	2.0610	6.5043
18	1.4592	5.2393	1.4776	4.7995
19	1.2696	3.9245	1.2305	3.4036
20	0.9988	2.9136	0.9250	2.3690
21	0.8265	2.2486	0.7235	1.7022
22	0.6255	1.9275	0.5303	1.4064
23	0.4629	1.5370	0.3918	1.0958
24	0.3227	1.1219	0.2712	0.7386
25	0.2451	0.8569	0.2176	0.5743
26	0.1707	0.7733	0.1600	0.4999
27	0.1368	0.6165	0.1296	0.4275
28	0.0937	0.6079	0.0980	0.3745
29	0.0625	0.4312	0.0658	0.3048
30	0.0428	0.4356	0.0461	0.2410
31	0.0253	0.3958	0.0310	0.2329
32	0.0159	0.3053	0.0182	0.1759
33	0.0085	0.2830	0.0106	0.1595
34	0.0070	0.3259	0.0054	0.1325
35	0.0425	0.1648	0.0033	0.1384
MW	202.9		201.3	

Table 3
Amount of solid paraffin for samples 1 and 2 for each temperature measured (mass %). The relative expanded uncertainty is 5% of the presented value.

Temperature (K)	Sample 1	Sample 2
273.75	0.29	0.26
268.15	0.68	0.52
263.15	1.37	1.14

$$A_{1l} = -(6.99724 - 8.69326Kw_l + 0.27715Kw_l^2) \times 10^{-4} \quad (27)$$

$$A_{2l} = -2.2582 \times 10^{-6} \quad (28)$$

$$B_{0l} = 1.09223 - 2.48245\omega_l \quad (29)$$

$$B_{1l} = -(3.434 - 7.14\omega_l) \times 10^{-3} \quad (30)$$

$$B_{2l} = -(7.2661 - 9.2561\omega_l) \times 10^{-7} \quad (31)$$

$$C_l = \left[\frac{(12.8 - Kw_l)(10 - Kw_l)}{10\omega_l}\right]^2 \quad (32)$$

Kw is the Watson factor [17], defined by Eq. (33), in which the boiling temperatures of the pseudocomponents, T_b, were obtained from the work of Katz and Firoozabadi [13]. The specific gravity at 15.5 °C, SG, is approximately equal to the density, ρ, of the component, which is also obtained from Katz and Firoozabadi [13].

$$Kw_l = \frac{\sqrt[3]{1.8T_{bl}}}{SG_l} \quad (33)$$

For the solid phases, the thermodynamic path used to calculate the

Viance Exhibit 1068
Viance v. Koppers Performance Chemicals
PGR2026-00023
Page 4 of 8

Table 4
Compositions of solid paraffins of sample 1 in mass fractions for each temperature evaluated. The relative expanded uncertainty is 5% of the presented value.

Carbon Number	Temperature (K)		
	273.75	268.15	263.15
19	–	0.009	0.018
20	–	0.011	0.050
21	–	0.034	0.087
22	0.017	0.061	0.128
23	0.043	0.108	0.154
24	0.077	0.131	0.137
25	0.118	0.147	0.120
26	0.140	0.132	0.092
27	0.151	0.115	0.072
28	0.132	0.084	0.049
29	0.116	0.068	0.038
30	0.073	0.038	0.021
31	0.054	0.027	0.015
32	0.031	0.014	0.008
33	0.020	0.009	0.005
34	0.012	0.006	0.003
35	0.016	0.006	0.003

Table 5
Compositions of solid paraffins of sample 2 in mass fractions for each temperature evaluated. The relative expanded uncertainty is 5% of the presented value.

Carbon Number	Temperature (K)		
	273.75	268.15	263.15
19	–	–	0.013
20	–	–	0.051
21	–	0.011	0.073
22	0.010	0.024	0.097
23	0.022	0.079	0.134
24	0.040	0.093	0.125
25	0.081	0.128	0.123
26	0.117	0.143	0.099
27	0.151	0.141	0.086
28	0.148	0.117	0.063
29	0.144	0.100	0.053
30	0.097	0.059	0.030
31	0.076	0.044	0.022
32	0.045	0.024	0.013
33	0.029	0.016	0.008
34	0.018	0.010	0.005
35	0.022	0.011	0.005

Table 6
Parameters obtained that multiply the pseudocomponent molecular weights, ξ_{MW}, boiling, ξ_{T_b}, and critical, ξ_{T_c}, temperatures and the paraffins' pair interaction energies, ξ_λ.

Diesel	ξ_{MW}	ξ_{T_b}	ξ_{T_c}	ξ_λ
1	0.9932	1.126	0.7372	0.9935
2	1.026	1.139	0.8011	0.9906

molar enthalpy goes through the liquid phase, for which the description above holds. It then proceeds by taking into consideration the effect of the heat capacities of the liquid, the solidification of the liquid, the solid-solid phase transition, the effect of the heat capacities of the solid and, finally, the excess enthalpy, h^E, so that a solid phase mixture is considered. As such, neglecting the effects of pressure changes, Eq. (34) is used to calculate the molar enthalpies of solid phases, h^S.

$$h^S(T,P,\underline{x}^S) = \sum_{i=1}^{N_c} x_i^S \left[\int_{T_0}^{T} Cp_i^{ig} dT - \int_{T_i^{fus}}^{T} \Delta Cp_i^{LS} dT - \Delta h_i^{fus} - \Delta h_i^{tr} \right] + h^R(T,P,\underline{x}^S) + h^E(T,\underline{x}^S) \quad (34)$$

The total molar enthalpy of the system is calculated by summing over the number of phases, N_p, the product between the molar enthalpy of the phase and its respective molar phase fraction, β, as presented in Eq. (35).

$$h = \sum_{j=1}^{N_p} \beta^j h^j \quad (35)$$

The heat flow, $\delta Q/\delta t$, is obtained using Eq. (36), in which the number of moles of the sample, N_{mol}, and the variation of T with time, $\partial T/\partial t$, are similar to the experimental ones. The variation of the total molar enthalpy of the system with the temperature, $\partial h/\partial T$, is calculated numerically.

$$\frac{\delta Q}{\delta t} = \frac{\partial h}{\partial T}\frac{\partial T}{\partial t} N_{mol} \quad (36)$$

3.3. Thermogram fitting

To adjust the model to the experimental DSC thermograms, the pseudocomponents properties, ideal gas heat capacities and molecular weights were tuned, as well as the pair interaction energy parameter, λ_{ij}, from the solid model. The initial guesses of all pseudocomponent properties were obtained from Katz and Firoozabadi [13].

To limit the number of tuning parameters, instead of adjusting each property of each pseudocomponent, a single multiplier was used to

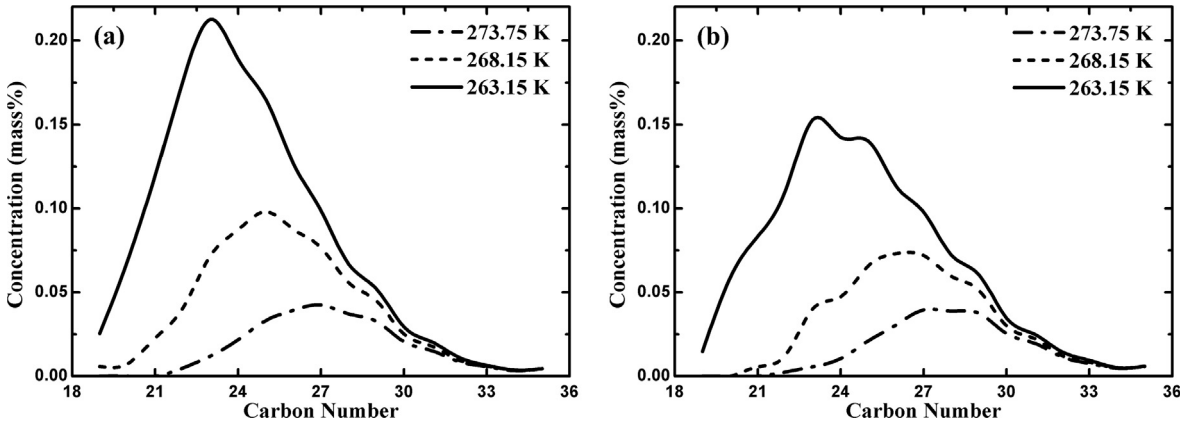

Fig. 1. (a) Concentration of the paraffins in the solid for different temperatures from sample 1. (b) Concentration of the paraffins in the solid for different temperatures from sample 2.

Viance Exhibit 1068
Viance v. Koppers Performance Chemicals
PGR2026-00023
Page 5 of 8

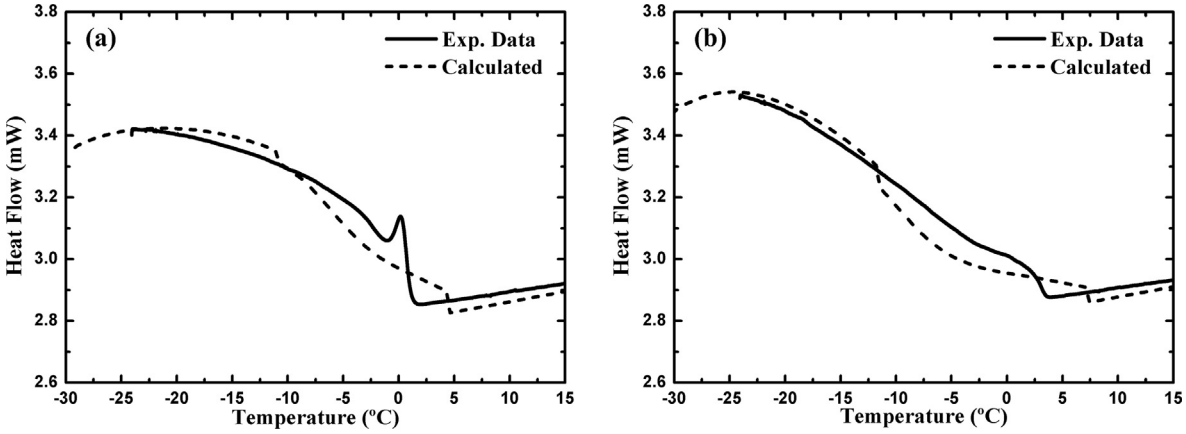

Fig. 2. Experimental and fitted DSC curves for Diesel 1 (a) and Diesel 2 (b).

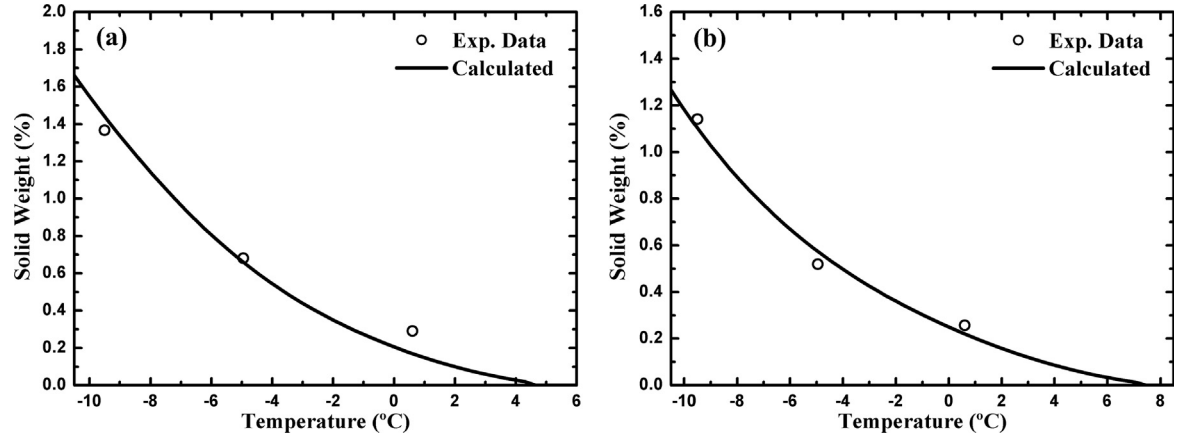

Fig. 3. Experimental and predicted solubility curves for Diesel 1 (a) and Diesel 2 (b).

adjust simultaneously each of the properties for all pseudocomponents. In this way, only four multipliers were tuned to fit the calculated thermogram to the experimental thermogram.

The molecular weights of the pseudocomponents were the first parameters adjusted using the multiplier ξ_{MW}. The molecular mass of the sample was tuned to its measured average molecular weight, presented in Table 2.

The other pseudocomponent properties were adjusted by fitting the simulated thermogram to the experimental DSC thermogram in three steps. The first step was to estimate the parameter ξ_{T_b} that multiplies the pseudocomponents boiling temperatures. These boiling temperatures are used to calculate their ideal gas heat capacities by Eqs. 25–27, 32 and 33. As the thermogram recorded at temperatures higher than the WAT are only a function of the heat capacity of the sample and thus a direct function of the ideal gas heat capacities of the samples components, this region was used to tune ξ_{T_b}.

The second step was to estimate the parameter ξ_{T_c} that multiplies the pseudocomponents critical temperatures. This parameter was estimated using the thermogram region ranging from 5 °C below the WAT to the lowest temperature measured.

A final adjustment to the solid-liquid equilibrium curve, the third step, was performed by estimating a parameter ξ_λ that modifies the paraffin pair interaction energies, as proposed by Silva et al. [9]. In this work, ξ_λ is equal to $(1 + \Delta\lambda)$ from Silva et al. [9]. This estimation was carried out using the same region used in step 2. Tests showed that iteration of this sequential parameter estimation is not necessary, since its computational cost is very high and a minor accuracy gain is achieved.

In all three steps described, the objective function was the RMSD between the simulated and the experimental thermograms for each of the regions of interest.

3.4. Solid-liquid equilibrium prediction

From the model with the tuned parameters, the so-called wax appearance temperature that correspond in fact to the wax disappearance temperature can be predicted by calculating the solid-liquid phase transition temperature at fixed pressure. This temperature cannot be determined by calorimetric measurements due to subcooling effects. In addition, the model allows calculating of solid-liquid phase equilibrium condition below the wax appearance temperature by solving Eq. (1). This phase equilibrium calculation provides the amount of solid deposit as well as its composition as a function of temperature.

4. Results and discussion

The feed compositions of both samples 1 and 2 in terms of paraffins and pseudocomponents are presented in Table 2.

The amounts of solids measured at various temperatures below the wax appearance temperature in order to build the solubility curve are presented in Table 3. The compositions of the solid paraffin at each temperature for sample 1 are presented in Table 4 and those for sample 2, Table 5.

The compositions of the solid phases in respect to the original sample mass for both samples are shown in Fig. 1. As can be seen, at higher temperatures, the solids are composed majorly by the heavy paraffins. As temperature decreases, the lighter paraffins start to incorporate into the solid. Nevertheless, even at the highest temperature,

Viance Exhibit 1068
Viance v. Koppers Performance Chemicals
PGR2026-00023
Page 6 of 8

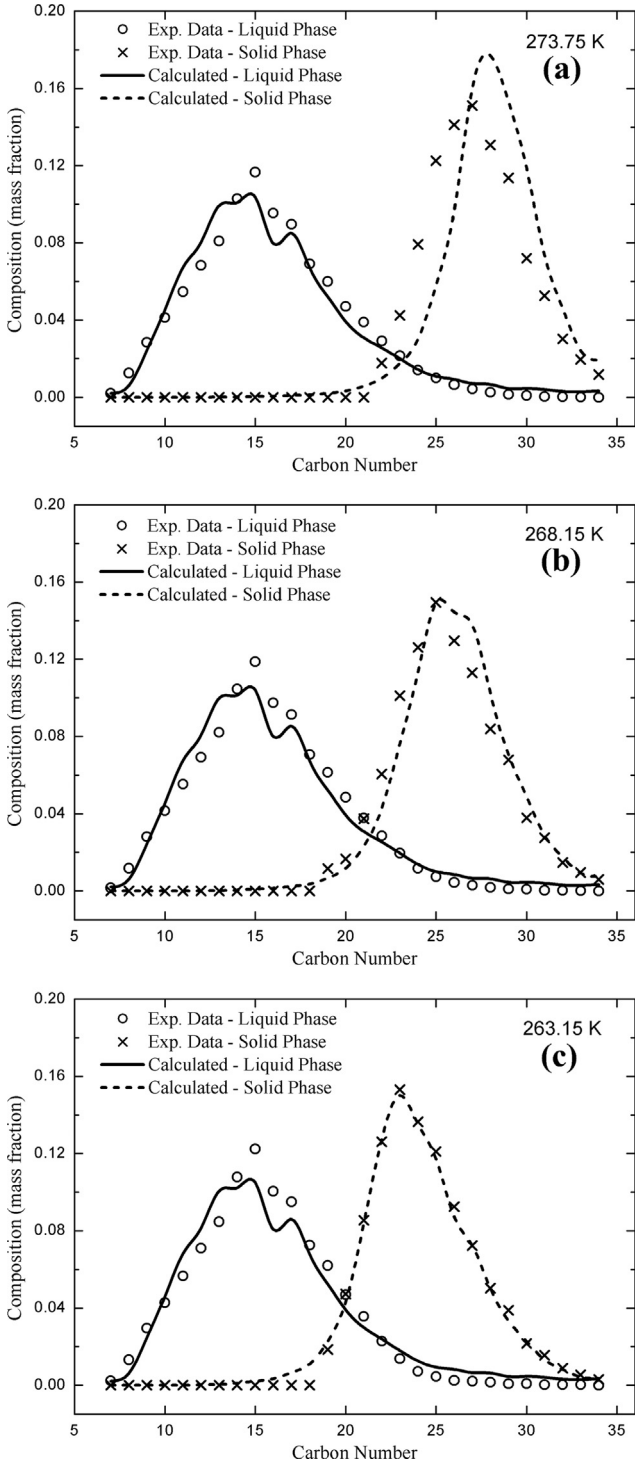

Fig. 4. Experimental and predicted compositions of liquid and solid phases at 273.75 K (a), 268.15 K (b) and 263.15 K (c) for Diesel 1.

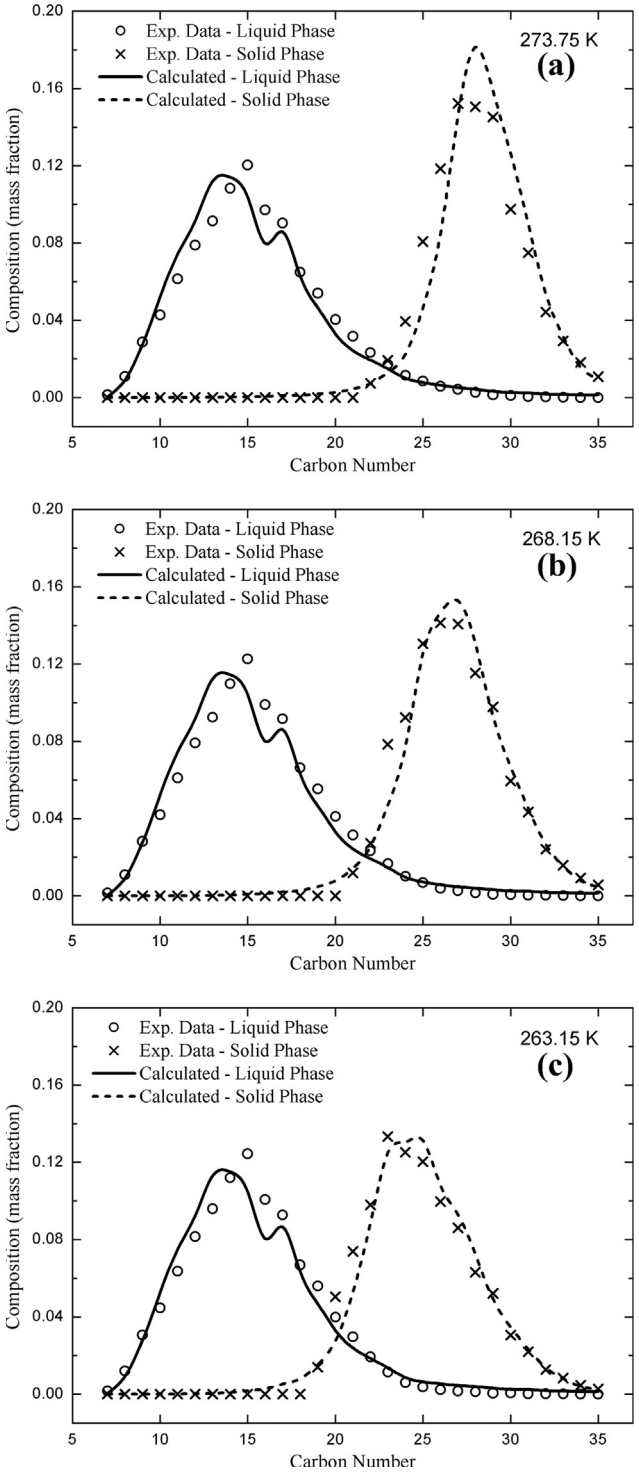

Fig. 5. Experimental and predicted compositions of liquid and solid phases at 273.75 K (a), 268.15 K (b) and 263.15 K (c) for Diesel 2.

the composition spreads over a big number of paraffins, suggesting that the solid consists of a solid solution of paraffins rather than a simple mixture of pure single paraffin solids.

The results obtained for the tuning multipliers are depicted in Table 6. The molecular weight multiplier, ξ_{MW}, corrects the pseudo-components molecular weight by just 2.6% at most. This correction is within the experimental uncertainty of the measured molecular weight. Moreover, the parameters ξ_{λ} modify the pair interaction energies in less than 1%, what is in agreement with results presented by Silva et al. [9].

The results for the calculated thermogram for both samples after the tuning are presented in Fig. 2. As can be seen, tuning the model to the rest of the thermogram instead of just to the WAT leads to a difference between the experimental DSC WAT and the solid-liquid equilibrium temperature calculated. The experimental limitations lead to an experimental WAT lower than the crystallization temperature predict by the model, as shown in Fig. 2. Actually, due to subcooling of paraffins and kinetic effects during experiments carried out by cooling, scanning calorimetry experiment does not give access to the real WAT. The proposed methodology based on fitting the full thermogram provides a

Viance Exhibit 1068
Viance v. Koppers Performance Chemicals
PGR2026-00023
Page 7 of 8

more realistic WAT value by correcting this drawback.

The experimental solubility curves for both samples as well as the calculated curves are presented in Fig. 3. As can be seen, the differences are smaller than the experimental uncertainties. To further compare experimental results and the model, the solid and liquid phases compositions for each sample at each temperature are shown in Figs. 4 and 5. Again, the simulated results are in very good agreement with the experimental data for all cases analyzed.

It seems natural that the solubility curves were well represented by the proposed methodology based on fitting DSC measurements as the area of the thermogram peaks are directly related to the amount of waxy solid formed. In contrast, no composition information of the liquid and solid phases measured were used to fit the model and yet the comparison between them and their predictions agree to within experimental uncertainties. This last result, above all, indicates the soundness of the model and clearly shows the predictive capacity of the developed fitting procedure.

The proposed methodology presents itself as a robust alternative to tune thermodynamic solid-liquid equilibria models. The final uncertainty is smaller when compared to the alternative of tuning the model to one temperature alone, the WAT. It also allows the tuning of models to more complex fluids, like crude oil, as long as DSC thermogram at a slow enough rate is available.

5. Conclusion

Solid precipitation in Diesel fluids driven by low temperatures is at the heart of many problems regarding systems that run on this fuel. To assess the risks of a given sample, thermodynamic solid-liquid equilibria models are employed. These thermodynamic models are tuned using the wax appearance temperature, WAT, the highest temperature at which a first crystal of paraffin is spotted in a cooling experiment.

A new strategy to tune thermodynamic solid-liquid equilibria models has been recently proposed [8,9]. It consists of using DSC thermograms instead of the WAT to adjust the model to experimental data. The strategy has been tested for standard mixtures with well known composition and in this work it is tested against real mixtures where the whole composition is not available. Two different Diesel fuel samples supplied by PETROBRAS are analyzed and their phase behavior assessed by a thermodynamic model.

Calorimetric data ranging from 248.15 K to 303.15 K and solubility data at 273.75 K, 268.15 K and 263.15 K were measured for the two samples. The solid-liquid phase equilibria behavior of these samples were modeled using the PR-EoS for the liquid phase and the modified UNIQUAC model for the solid phase. The models were fitted to the DSC data aiming to correctly reproduce the solubility data and, to do that, the simulated heat flows were calculated according to the methodology proposed by Silva et al. [9]. A parameter estimation was employed, in which the pseudocomponents molecular weights are tuned to the average molecular weight of the samples, followed by the fitting of the simulated thermograms to the DSC experimental results by tuning the pseudocomponents boiling and critical temperatures and the paraffin pair interaction energies, in this order.

The results were in agreement to both the DSC and solubility experimental data for both samples. The solid phase simulated and experimental compositions were in very good agreement for the two samples. The same holds for liquid phases. This way, the developed methodology proves to perform very well for real complex samples.

Acknowledgements

The authors acknowledge PETROBRAS for the Diesel fuel samples and ANP-PETROBRAS program for the financial support. R. P. do Carmo and F. W. Tavares thank CAPES and CNPq. The authors also acknowledge Juliana Tamanqueira, Bruno do Couto, Daniele Gonçalves and Klaire Paes for all the help given over the chromatographic analyzes.

References

[1] Coutinho JAP. A thermodynamic model for predicting wax formation in jet and diesel fuels. Energy Fuels 2000;14:625–31.
[2] Maithufi MN, Joubert DJ, Klumperman B. Application of gemini surfactants as diesel fuel wax dispersants. Energy Fuels 2011;25:162–71.
[3] Zheng W, Wang S, Liu J, Meng F, Li Y, Ma H, et al. Synthesis and evaluation of wax dispersant for diesel. Energy Fuels 2014;28:1896–900.
[4] Coutinho JAP, Mirante F, Pauly J. A new predictive UNIQUAC for modeling of wax formation in hydrocarbon fluids. Fluid Phase Equilib 2006;247:8–17.
[5] Sansot JM, Pauly J, Daridon JL. Modeling high-pressure wax formation in petroleum fluids. AIChE J 2005;51(7):2089–97.
[6] Coutinho JAP, Dauphin C, Daridon JL. Measurements and modelling of wax formation in diesel fuels. Fuel 2000;79:607–16.
[7] Coutinho JAP, Daridon JL. The limitations of the cloud point measurement techniques and the influence of the oil composition on its detection. Pet Sci Technol 2005;23:1113–28.
[8] Fleming FP, Daridon JL, Azevedo LFA, Pauly J. Direct adjustment of wax thermodynamic model parameter to Micro Differential Scanning Calorimetry thermograms. Fluid Phase Equilib 2017;436:20–9.
[9] Silva VM, Carmo RP, Fleming FP, Daridon J, Pauly J, Tavares FW. Paraffin solubility and calorimetric data calculation using Peng-Robinson EoS and modified UNIQUAC models. J Petrol Sci Eng 2017;156:945–57.
[10] Han S, Huang Z, Senra M, Hoffmann R, Fogler HS. Method to determine the wax solubility curve in crude oil from centrifugation and high temperature gas chromatography measurements. Energy Fuels 2010;24(3):1753–61.
[11] Marano JJ, Holder GD. General equation for correlating the thermophysical properties of n-paraffins. n-olefins. and other homologous series. 2. Asymptotic behavior correlations for PVT properties. Ind Eng Chem Res 1997;36:1895–907.
[12] Pedersen KS, Christensen PL. Phase behavior of petroleum reservoir fluids. Boca Raton: CRC Press, Taylor & Francis Group; 2007. 81-113.
[13] Katz DL, Firoozabadi A. Predicting phase behavior of condensate/crude-oil systems using methane interaction coefficients. J Petrol Technol 1978;30:1649–55.
[14] Morgan DL, Kobayashi R. Extension of Pitzer CSP models for vapor pressures and heats of vaporization to long-chain hydrocarbons. Fluid Phase Equilib 1994;94:51–87.
[15] Pedersen KS, Skovborg P, Ronningsen HP. Wax precipitation from north sea crude oils 4. Thermodynamic modeling. Energy & Fuels 1991;5(6):924.
[16] Passut CA, Danner RP. Correlation of ideal gas enthalpy, heat capacity, and entropy. Ind Eng Chem Process Des Develop 1972;11:543–6.
[17] Kesler MG, Lee BI. Improve prediction of enthalpy of fractions. Hydrocarbon Process 1976;55:153–8.

Viance Exhibit 1068
Viance v. Koppers Performance Chemicals
PGR2026-00023
Page 8 of 8